Cement and Concrete Composites 138 (2023) 104981

Contents lists available at ScienceDirect

Cement and Concrete Composites

journal homepage: www.elsevier.com/locate/cemconcomp

The effect of fibres and carbonation conditions on the mechanical properties and microstructure of lime/flax composites

A. Rakhsh Mahpour [a], H. Ventura [b,c], M. Ardanuy [b,c,*], J.R. Rosell [a], J. Claramunt [d]

[a] Department of Architectural Technology, Universitat Politècnica de Catalunya, Doctor Marañón, 44-50, 08028, Barcelona, Spain
[b] Department of Materials Science and Engineering, Textile Division, Universitat Politècnica de Catalunya, Colom, 1, 08222, Terrassa, Spain
[c] Institute of Textile Research and Industrial Cooperation of Terrassa, Universitat Politècnica de Catalunya, Colom, 15, 08222, Terrassa, Spain
[d] Department of Agri-Food Engineering and Biotechnology, Universitat Politècnica de Catalunya, Esteve Terradas, 8, 08860, Castelldefels, Spain

ARTICLE INFO

Keywords:
Textile-reinforced composites
Lime composites
Historical building reinforcement
Mechanical properties
Microstructure

ABSTRACT

Fibre and textile-reinforced mortars are increasingly being used for a variety of building applications, including the strengthening of masonry structures. Lime mortars reinforced with sustainable fibres (such as vegetable or cellulosic fibres) may provide an interesting solution. In this paper, a mixture of commercial lime with 20% metakaolin addition was used to produce composites reinforced with non-woven flax fabrics that were cured at different moisture contents (from 0 to 100%) for 7 or 14 days in a CO_2 incubator. The composites were characterised to determine their flexural behaviour, carbonation level and microstructure. According to the results, no differences exist in the flexural strength of the composites made in the moisture range of 33%–66%. At 7 days of curing, they attained Modulus of Rupture (MOR) values that exceeded 5.5. MPa. Moreover, it was observed that under high moisture conditions, the permeability of the fibres allows for CO_2 access, despite the saturation of the pores of the matrix – allowing a reaction in the vicinity of the fibres –, while under dry conditions, the fibre's moisture retention does not permit the carbonation of the matrix in their vicinity, even though complete carbonation takes place after 14 days.

1. Introduction

Over recent decades, one of the most common methods of retrofitting masonry structures has been the use of fibre-reinforced polymers (FRPs) in the form of laminates, sheets, or rods. FRPs are composite materials in which a polymer matrix (typically epoxy, polyester, or vinyl ester resin [1]) is reinforced with relatively thin and long fibres. In civil engineering, the most commonly-used FRPs are those reinforced with carbon (CFRP) or glass (GFRP) fibres, which mainly differ in their stiffness and tensile strength. Despite their increasing popularity, certain drawbacks arise when strengthening structural elements with FRPs, mainly due to their limited fire resistance and high cost (including material and labour costs). Moreover, most FRPs are not suitable for strengthening historical constructions due to the incompatibility between the resin and the substrates. Thus, the use of inorganic materials as binders may prevent issues such as poor behaviour at high temperatures, vapour impermeability, or incompatibility with masonry substrate, among others. Hence, the use of inorganic binders (such as cement-based or lime-based mortars) provides more advantageous strengthening solutions than organic resins. Fibre- and textile-reinforced mortars (FRM and TRM, respectively) have been used to address the numerous drawbacks related to the use of FRP in the strengthening of unreinforced masonry walls [2,3].

As for the mortars used to reinforce historical buildings, it should be mentioned that the physical-mechanical features of cement-based mortars differ greatly from those of lime-based mortars in terms of brittleness, mechanical strength, vapour permeability, and thermal expansions (with cement mortars being more resistant and having a greater adhesion than lime mortars). However, historical buildings typically contain sensitive lime-based mortars and masonry works, which suffer from the negative effects of durability derived from retrofitting works with cement-based mortars. In many cases, this results in the cement layer tearing away some of the masonry material from the substrate. Moreover, from a chemical point of view, damage may arise as a result of the interaction between cement hydration products and certain building stones, as recently observed with clay bricks, for instance Ref. [4].

* Corresponding author. Department of Materials Science and Engineering, Textile Division, Universitat Politècnica de Catalunya, Colom, 1, 08222, Terrassa, Spain.
E-mail address: monica.ardanuy@upc.edu (M. Ardanuy).

https://doi.org/10.1016/j.cemconcomp.2023.104981
Received 21 October 2022; Received in revised form 7 January 2023; Accepted 7 February 2023
Available online 9 February 2023

Therefore, mortar must be considered as a sacrificial element that should be weaker than the masonry works, since preferably, this repair material should break before the original crafted bricks do [5]. Thus, the use of lime-based mortars may be more appropriate for this application.

However, certain challenges arise with the use of lime-based mortars since, like other traditional materials, they tend to crack due to the undesired plastic shrinkage resulting from rapid water evaporation, especially in dry environments. In cement- or lime-based materials, the use of fibrous reinforcements has helped to reduce plastic shrinkage and jointly enhances mechanical properties and durability [6,7]. For instance, the addition of reinforcing fibres has been found to improve tensile and flexural strength, ductility, toughness and long-term effects, while also being compatible with the original matrix [8]. Nevertheless, both increases and decreases in compressive strength are recorded when fibres are added. It has been suggested that the decrease in strength may be due to the increase of the mixture in the air content, as compared to plain mortar, while the increase in strength is a result of the fibres being positioned horizontally, stitching the micro-cracks and bridging the matrix cracks, and transferring the loads [9,10].

In recent years, the use of more sustainable and environment-friendly fibres in FRM/TRM has become more common. For general building applications, vegetable and recycled fibres in different short or long forms, as well as woven and non-woven textile forms, have been used to reinforce cementitious matrixes, especially for low-to-medium performance structural applications [10–15]. Non-woven fabrics are planar engineered fibrous assemblies in which the fibres have been consolidated or entangled by physical or chemical means to provide certain level of structural integrity. They reveal a lower porosity and are cheaper option when compared to the open-structure woven fabrics typically used for cementitious reinforcement [16]. In fact, only few studies use non-woven fabrics for the reinforcement of cement-based composites [17–20], and even fewer studies in the literature have examined the use of flax fibres as reinforcement in lime-based mortars for their application as strengthening materials in historical buildings [7]. Nonetheless, to the best of our knowledge, the use of non-woven flax fabrics as reinforcement structures in lime composites has not yet been studied.

It is widely known that in lime pastes, after its cohesion derived from the loss of water, the hardening takes place through the carbonation process of $Ca(OH)_2$ where the reaction is necessary to produce the precipitation of $Ca(CO)_3$, leading to a material with strong chemical bonds and a higher strength. However, this natural carbonation at room temperature needs a long time to take place. Hence, the use of forced carbonation curing of lime mortars is highly motivated to shorten such a process. According to several studies [21–23], accelerated carbonation – which depends on the temperature, humidity, CO_2 pressure, and duration of the process – can reduce the time of carbonation significantly. Moreover, the incorporation of metakaolin (MK) can lead to the formation of calcium silicate hydrates (C–S–H) among other phases due to a pozzolanic reaction, which can improve the mechanical properties of these lime pastes [24,25].

This study, therefore, aims to contribute to the development of lime-based composites using non-woven flax fabric reinforcement to achieve the quality performance necessary for their application as a coating and/or a reinforcement of masonry walls. In this case, commercial lime (CL) pastes with 20% metakaolin (MK) were prepared with a water/binder ratio of 1.0 – optimised in a prior work [19] – for use as a matrix. With this paste, lime composite plates reinforced with six layers of non-woven flax fabrics were prepared. In order to study the effects of the fibre's presence and the carbonation conditions on the resulting composites, the plates were cured with different moisture contents (0%, 33%, 66%, and 100%) for 7 or 14 days in a CO_2 incubator. Then, the mechanical behaviour of the plates was determined using flexural tests. Finally, an optical microscopy, a backscattered (BSEM) electron microscopy and an EDS analysis were performed to examine the microstructure of the samples.

2. Experimental procedure

2.1. Materials

2.1.1. Matrix materials

A commercial lime (CL) – reference CL-90 supplied by *Dcal by Ciaries, SLU* (Olesa de Bonesvalls, Barcelona, Spain) – was used to produce the pastes. Its chemical composition and physical/mechanical properties are shown in Table 1.

The lime was mixed with 20% metakaolin (MK), supplied by *Arcillas Refractarias ARCIRESA, SA* (Gijon, Asturias, Spain) with the commercial name of metakaolin Peser. This is a product with high pozzolanic activity and has the physical and chemical characteristics presented in Table 2 (data provided by the manufacturer). This material was selected for aesthetic reasons (i.e. colour), to avoid modifying the lime tone since the developed composite is intended for use as a coating and/or a reinforcement in historical buildings and structures.

2.1.2. Reinforcement material

An optimised non-woven flax fabric was used as a composite reinforcement. The non-woven material was obtained using flax fibres with an average length of 60 mm, from a carding and needle-punching *DILO OUG-II-6* pilot plant (Fig. 1), as described in previous works [26,27].

Before producing the composites, the non-woven flax fabrics were subjected to wet/dry cycles (hornification process) to improve fibre-matrix adhesion and dimensional stability within the lime matrix [28–31]. The hornification treatment consisted of 4 wet-dry cycles, each initially being immersed in distilled water at room temperature for 6 h, followed by drying in an air-circulating oven at 60 °C for 24 h. Hornification treatment irreversibly modifies the fibres: the lumen collapses due to the formation of hydrogen bonds, and their surface roughness and dimensional (volumetric) stability against humidity variations are increased, while water absorption capabilities decrease, thus leading to an improved fibre/matrix adhesion and durability of the composite against wet-dry ageing [30–34].

The main characteristics of the non-woven fabric after the hornification treatment are presented in Table 3.

2.2. Composite plates preparation

2.2.1. Paste preparation

In a prior study [19], the water/binder (w/b) ratio and pozzolanic content were assessed to maximise both the penetrability of the matrix through the non-woven reinforcement and the mechanical behaviour of the matrix. One of the conclusions of this previous study was that improved mechanical properties are attained by adding 20% MK. Therefore, the matrix used in this study was prepared with an 80% CL, 20% MK and a w/b ratio of 1 by mixing the raw materials and the corresponding water amount with a *VELP LH* stirrer. The particle size distribution of the raw materials and the 80/20 mixture is provided in

Table 1
Physical-chemical properties of commercial lime CL-90 (data by the manufacturer).

Physical properties (CL 90)			Chemical Analysis (CL 90)		
	Specification[a]	Result		Specification[a]	Result
Free water (%)	≤2	0	Cao (%)	≥90	91
Stability Expansion (mm)	≤2	0	MgO (%)	≤2	0
Penetration (%)	>10 and <50	21	CO_2 (%)	≤5	2
Air content (%)	≤12	2	SO_3 (%)	≤4	0
Free water (%)	≤2	0	Free lime (%)	≥80	91

[a] According to UNE EN 459–1 2015.

Table 2
Physical-chemical properties of metakaolin Peser.

Physical properties		Chemical Analysis	
Appearance/color	White powder	% Al_2O_3	40.24
Loss on ignition	<1.5%	% SiO_2	54.61
Pozzolanicity (Chapelle test)	988 mg $Ca(OH)_2$/g	% Fe_2O_3	0.25
Specific surface (Blaine)	10.971 cm^2/g	% TiO_2	1.06
Water demand	106.2%	% CaO	<0.10
28-day resistant activity index	111.6%	% Na_2O	0.02
Apparent density (aired)	600 kg/m^3	% K_2O	1.44
Apparent density (compacted)	800 kg/m^3		
Specific weight	2540 kg/m^3		

Fig. 2. The flexural strength and flexural stiffness of the mentioned paste were 1.53 ± 0.26 MPa and 3.33 ± 81 MPa, respectively.

2.2.2. Layer stacking and moulding

Firstly, the non-woven fabrics were cut to the mould's internal dimensions (300 mm × 300 mm) and were then carefully impregnated into the paste and piled up in the mould. Six layers of impregnated reinforcement were stacked (alternating the orientation of each nonwoven layer in the machine- or cross-direction) and a thin paste layer on the top and bottom was added, creating a sandwich-like plate with a thickness of ~10 mm. The high w/b ratio permits a good penetrability of the paste since the reinforcement generates an excess of water that must be removed. To that end, the stacking process was vacuum assisted. Moreover, the specially designed mould allowed the application of a homogeneous pressure of 3.5 MPa for 24 h by means of an *Incotecnic* electromechanical press, helping to reduce the excess water. Once demoulded, the plates were kept in the laboratory, drying at room conditions for 7 days, in order to achieve their consolidation.

2.2.3. CO_2 plate curing

The sandwich-like structure of the composite material, defined by the layers of non-woven flax and the layers of the lime/metakaolin matrix, may influence the distribution of moisture and CO_2 diffusion into the material. Therefore, in order to determine the ideal carbonation conditions for the composite material, the consolidated plates were cut into 4 pieces of 150 mm × 150 mm. Each piece was conditioned to reach a specific state corresponding to the 4 different moisture contents were set for the study: 0%, 33%, 66%, and 100%. To obtain these different moisture contents, the pieces were first oven dried at 60 °C until a constant weight was reached (considered as 0% moisture content). Then, the pieces were submerged in water until reaching a constant weight (considered the 100% moisture content). Afterwards, the weight required to achieve the 33% and 66% conditions was calculated, and the corresponding pieces were dried accordingly from the saturated state until reaching the expected weights. The samples were sealed in a plastic bag to maintain the established moisture conditions until the carbonation process began.

The carbonation of the composite plate pieces (Fig. 3b) was carried out in the autoclave shown in Fig. 3a. The procedure consisted of an initial extraction of the air inside the chamber by means of a vacuum pump and then an injection of CO_2 gas until reaching a pressure of 0.20 MPa (2 atm), which was maintained throughout the carbonation process. To determine the optimal carbonation time, half of the samples were autoclaved for 7 days and the other half for 14 days. The designation of the samples was based on the curing days and the moisture content, as shown in Table 4.

2.3. Analysis of the composite plates

2.3.1. Mechanical characterisation

To evaluate the mechanical performance of the composite samples, three-point bending tests were performed on specimens of 150 mm × 50 mm × ~10 mm cut from the cured pieces. A total of 4 specimens per sample were tested in a *TA.XT plus texturometer* equipped with a load cell

Table 3
Physical and mechanical properties of the hornified non-woven flax fabric.

Physical properties		Mechanical properties	
Areal weight (GSM)	190 g/m^2	Tensile strength[a]	3.70 ± 1.41 N/g
Thickness	0.95 mm		

[a] Weight-normalized.

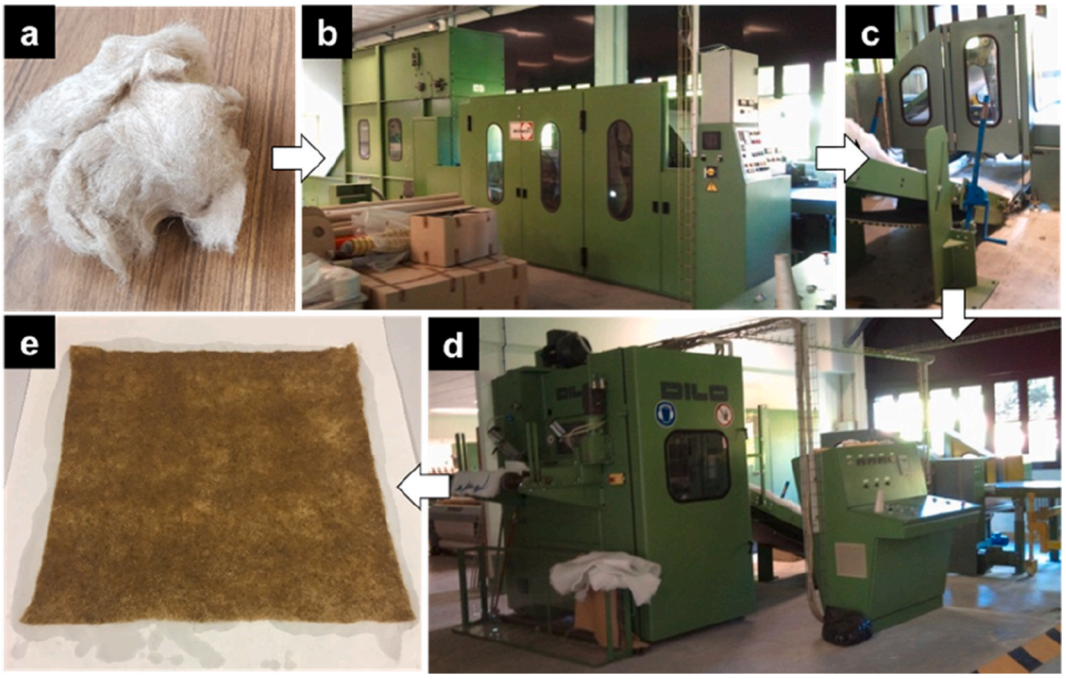

Fig. 1. Non-woven production system: (a) flax fibres; (b) fibre opening and carding unit; (c) cross-lapping unit layering the web; (d) needle-punching unit; and (e) non-woven material after wetting during the hornification process.

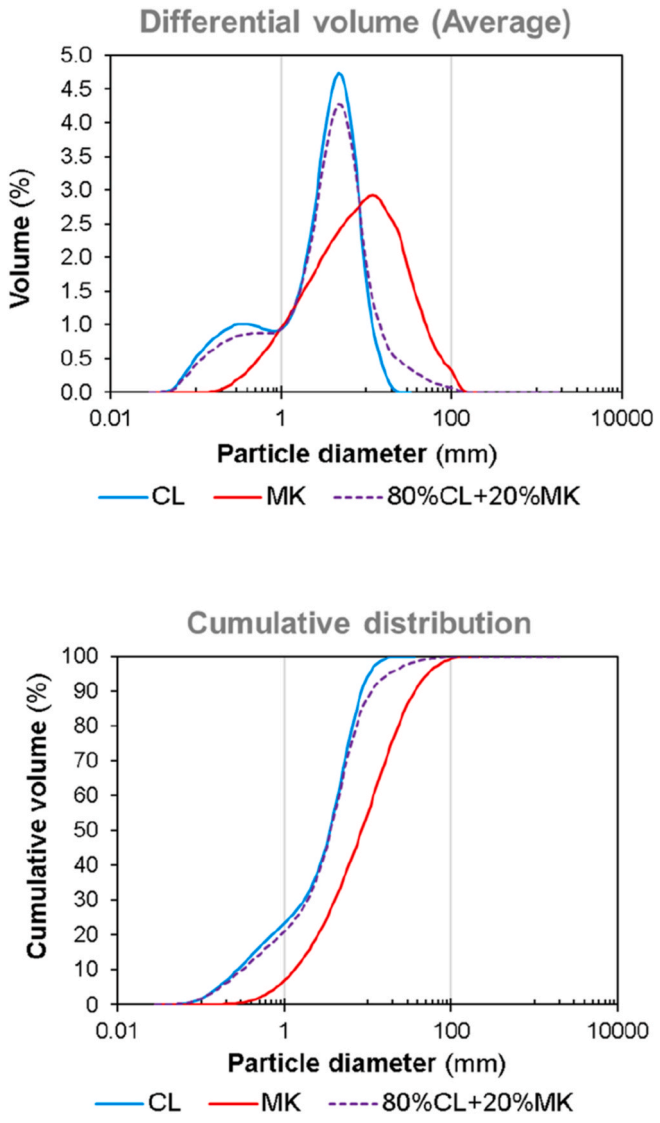

Fig. 2. Particle size distribution of the CL and MK raw materials, and their 80% CL and 20% MK mixture.

of 0.5 kN, at a loading rate of 6 mm/min with a bending span of 120 mm between the bottom supporting pins. Four parameters were determined and analysed from these flexural tests.

The limit of proportionality (LOP) – defined as the flexural stress value producing the first crack in the material – is determined upon the initial decline in the slope of the load/deflection diagram. This value is considered to be the matrix's threshold strength value and the point at which the reinforcing effect of the fibres begins.

The flexural strength or MOR (modulus of rupture) – defined as the maximum strength of the material – is determined for a 3-bending point configuration, as defined in Equation (1), where F (force) is the maximum load, l is the span length between the bottom anvils, b is the width of the specimen, and h is the specimen's thickness [10].

$$MOR\ (MPa) = \frac{3 \bullet F \bullet l}{2 \bullet b \bullet h^2} \tag{1}$$

The modulus of elasticity (MOE), for the configuration of this test, was determined according to Equation (2), where F_1 and F_2 correspond to two arbitrary loads in the elastic region of the curve and f_1 and f_2 correspond to the displacements (mid span deflection) produced by F_1 and F_2, respectively [10].

$$MOE = \frac{(F_2 - F_1) \bullet l^3}{4 \bullet (f_2 - f_1) \bullet b \bullet h^3} \tag{2}$$

Finally, the toughness index (I_G) consists of the area under the load-displacement curve comprised from zero to a deflection higher than 10% of the span (12 mm in this case), or to a post-failure load of the deformation value corresponding to 40% MOR (if such a limit occurs first) divided by the area of the specimen's transversal section. The I_G was established as the reference parameter to characterise the type of failure (ductile or fragile) and the post-failure deformation capacity.

In all cases, the results were analysed using an ANOVA with Tukey test group separation, with a significance value of 0.05.

2.3.2. Microstructural analysis

To reveal the extent of the carbonation process, specimens were cut and then, the internal sections were treated with a phenolphthalein solution. This indicator solution coloured the areas with a high pH level in a purplish tone that was then observed by optical means using a Nikon stereo microscope model SMZ 745. The purple areas corresponded to non-carbonated parts (rich in $Ca(OH)_2$ or C–S–H).

For a more in-depth analysis of the microstructure and composition of the lime-based matrix, the selected samples were cut to 10 mm × 5 mm × 5 mm using a diamond disk that was lubricated with isopropyl alcohol, further encapsulated in epoxy resin, polished to a roughness of 1 μm and sputtered with an 80/20 platinum/palladium alloy. Then, BSEM and EDS analyses were performed using a *JEOL JSM 7001F* model scanning electron microscope equipped with an *Oxford Instruments X-Max* energy dispersive X-ray spectrometer (EDS).

3. Results and discussion

3.1. Flexural behaviour of the lime-based composite plates

In Fig. 4, two examples of the specimen breakage are represented, revealing the relevance of the penetrability of the matrix through the nonwoven reinforcement. When the penetrability is poor, specimens present horizontal cracking related to a certain delamination, since the fibre/matrix adhesion does not allow a good shear-stress transfer (Fig. 4a). On the other hand, when the penetrability is successfully achieved, specimens present a clear multiple cracking transversal breaking pattern (Fig. 4b), leading to the breakage by matrix disaggregation combined with the fibre pull out of the reinforcement owing to fabric slippage. As expected, this multiple cracking is revealed in the stress vs deflection curves as numerous peaks, which denotes a good embedding of the nonwoven layers in the matrix.

In Fig. 5, the flexural stress vs mid-span deflection curves of the samples under study are plotted. The curves reveal the plastic behaviour of the material, and the mid-span deflection exceeds the limit of the specific energy defined in the RILEM TRF4 [35], which, in this case, is 12 mm. As can be seen, the curves begin with a linear region of high rigidity that corresponds to the behaviour of non-cracked material. Taking into account that the stiffness of the reinforcement is much lower than that of the lime matrix, this region is mainly dominated by the matrix properties. After this, the curve transitions towards a region with a lesser slope, related to a progressive reduction of the specimen's cross-section due to multiple cracking that leads to a loss of the load-bearing capacity. The multiple cracking is translated as numerous peaks in the curve, where the abrupt drops correspond to deeper cracks, implying a sudden reduction in aforementioned load-bearing capacity that is further recovered as a result of the reinforcing effect of the fibres. After this region, a plateau phase appears, mainly corresponding to the opening and growth of the cracks generated in the previous phase. At this point, the matrix gradually disintegrates while the material is bending. However, thanks to the tenacity of reinforcement layers – with the fibres structured in the nonwoven fabric –, the specimen does not

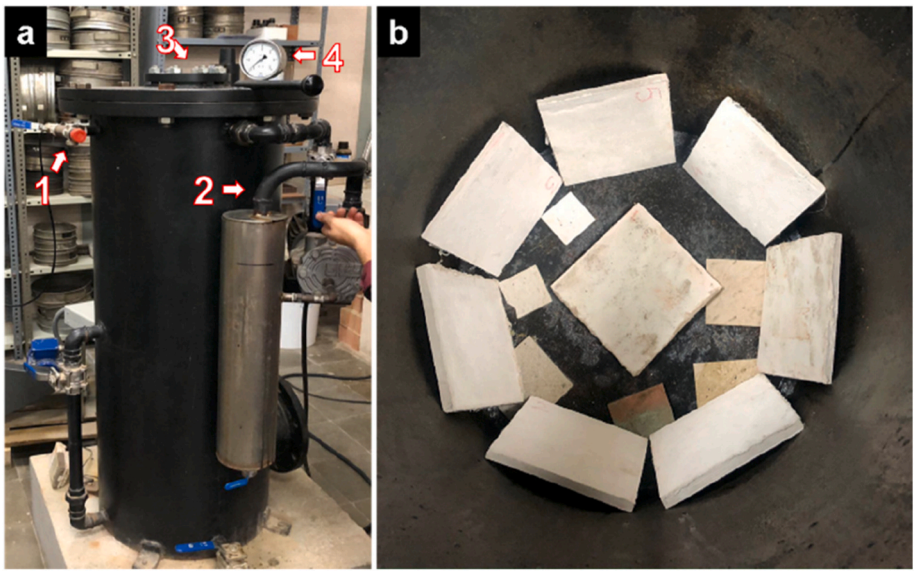

Fig. 3. a) Equipment used for the carbonation of the composite plates (custom autoclave) showing: 1) CO_2 injection valve, 2) vacuum pumping system, 3) peephole, and 4) chamber pressure control manometer. b) Samples placed inside the pressure vessel.

Table 4
Curing conditions for the composite samples (all performed at high CO_2 concentration).

Sample ref.	Curing time (days)	Moisture content (%)	Sample dry weight (g)	Water weight[a] (g)
CLMK/Flax-0/7	7	0	275.96	0
CLMK/Flax-33/07		33	291.89	31.45
CLMK/Flax-66/7		66	325.84	62.89
CLMK/Flax-100/7		100	370.30	94.34
CLMK/Flax-0/14	14	0	246.16	0
CLMK/Flax-33/14		33	320.30	47.88
CLMK/Flax-66/14		66	351.30	95.77
CLMK/Flax-100/14		100	389.81	143.65

[a] Determined as the difference between the samples' wet and dry weights.

split immediately. Only after a clearly noticeable stretching, the nonwoven layers slip and pull out, leading to a split of the specimen into two parts. This high deformability – found in all samples, regardless of the curing moisture content or curing time – denotes a good adhesion between the fibres and the matrix. Moreover, the curves reveal the strain-hardening behaviour of the composites.

However, Fig. 5 also shows the clear differences in the maximum flexural stress values reached by the samples with intermediate moisture contents (33% and 66%), and those with extreme moisture contents (0% and 100%), regardless of the curing time. This can be related to the degree of carbonation attained by the composites. As will be explained in section 3.2, the samples with intermediate moisture contents were fully carbonated, whereas samples with extreme moisture contents had some non-carbonated areas. To provide an accurate analysis of the flexural behaviour, the mechanical parameters extracted from the tests are summarised in Table 5. In all cases, the results were analysed using an ANOVA with a significance value of 0.05. To better compare the results, a separation by groups was carried out using a Tukey test, were one or more letters are assigned to each group (a, b, c, …) so that, when two groups do not have a common letter, it can be assured that they are significantly different.

Samples with a higher degree of carbonation develop a more resistant matrix (higher LOP and MOR values) which, in combination with the fibres, leads to a better general mechanical performance of the composite material. However, the reinforcement of the fibres leads to a higher effect of strength hardening in the samples having less carbonated matrices. This may be corroborated by the MOR/LOP ratios shown in Table 5, which were higher for samples having moisture contents of 0% and 100%, and lower for those with moisture contents of 33% and 66%.

As for the duration of the carbonation process, no significant differences were observed in the parameters except for the flexural modulus (MOE). Thus, samples with moisture contents of 0%, 66% and 100% revealed significantly higher stiffness when cured for 14 days, suggesting a certain increase in carbonation with time. According to these results, in terms of MOR, LOP and specific toughness (I_G), curing times of 7 days are sufficient to achieve optimal results, whereas, in terms of flexural modulus, 14 days of curing is preferable in order to attain higher values.

To summarise, the conditions required to obtain the CLMK/Flax-66/14 sample (curing with a 66% of moisture content for 14 days) result in the best overall mechanical performance. However, it is worth mentioning that the conditions required to obtain the CLMK/Flax-66/7 sample (curing with a 66% of moisture content for 7 days) may present a better trade-off between mechanical properties and production costs, given the good performance achieved, despite halving the carbonation process.

3.2. Microstructural analysis of the lime-based composite plates

3.2.1. Effect of fibres, moisture content, and curing time on the lime/flax composite carbonation

To analyse the behaviour of the material and the influence of the fibre's presence, the moisture content, and the curing time on the carbonation process, all of the composite samples cured in the CO_2 chamber were subjected to a phenolphthalein test.

In Fig. 6, the fibres appear as dark areas and the lime matrix is shown in white with purplish zones revealed by phenolphthalein. The latter indicates a high pH level, which is attributed to non-carbonated areas rich in calcium hydroxide or areas in which a pozzolanic reaction has taken place, resulting in high contents of hydrated calcium silicate

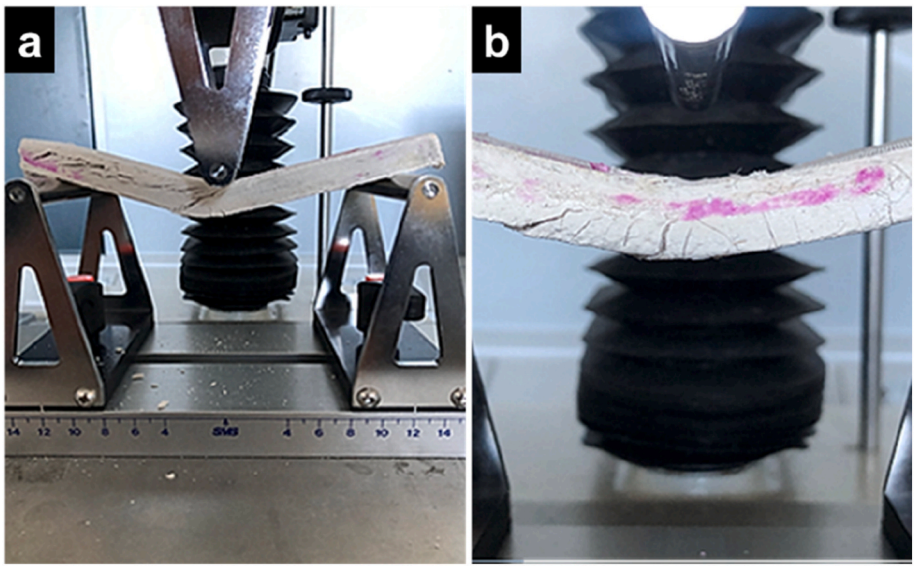

Fig. 4. a) Specimen breakage revealing delamination longitudinal cracks due to poor penetration of the matrix through the nonwoven reinforcement. b) Specimen breakage revealing a crack pattern associated to good matrix penetrability and good matrix/reinforcement adhesion.

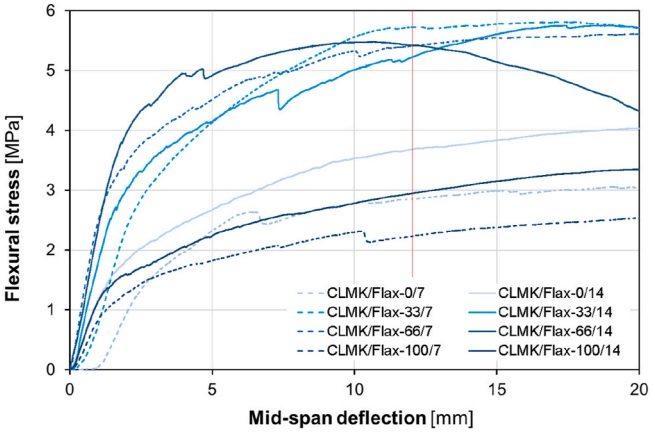

Fig. 5. Flexural stress vs mid-span deflection curves of the composite material cured with different moisture contents in a CO2 chamber for 7 and 14 days.

(C–S–H) phases. In both cases, the pH level of the aqueous solution remains above 9, within the indication range of phenolphthalein [36]. The areas that have not been dyed by the solution correspond to a lower pH level, which is typical of areas in which carbonation has occurred – in both calcium hydroxide and C–S–H – producing calcium carbonate with neutral pH [37,38].

Therefore, as seen in Fig. 6, the samples cured for 7 days with 33% and 66% moisture content, and those cured for 14 days with 0%, 33% and 66% moisture content presented very high or complete carbonation, whereas carbonation was not fully reached for the 100% moisture content sample cured for 14 days, or for the 0% and 100% moisture content samples cured for 7 days. These results are consistent with the mechanical properties observed and the corroboration observed may be attributed to the extent of matrix carbonation.

Moreover, in the samples cured for 7 days, in addition to the aforementioned differences between specimens with intermediate and extreme moisture contents, it can be observed that the specimens with 0% and 100% moisture contents have opposite carbonation imprints. Therefore, to improve the understanding of these results, an additional analysis was conducted, focusing on samples with extreme moisture contents that were cured for 7 days.

Fig. 7 shows the composite CLMK/Flax-0/7 (0% moisture content, top) and CLMK/Flax-100/7 (100% moisture content, down) specimens observed under optical microscopy with a magnification of 100×. Upon comparing these images, the opposite carbonation imprint can be clearly observed: for the sample with a low moisture content (0%), the non-carbonated part is found to surround the fibres, whereas for the sample with a high moisture content (100%), it is found in a reversed distribution (i.e. carbonated parts surround the fibres). This suggests that the presence of fibres alters the kinetics of the carbonation process, which is initiated at the central areas of the matrix when the moisture content is low, but at the areas surrounding the fibres when the moisture content is high.

To propose a hypothesis explaining this phenomenon, certain aspects of the carbonation reaction and the fibre's role should be considered.

In order to initiate the process, the carbonation reaction of the lime matrix typically requires the presence of CO_2 and humidity. CO_2 can diffuse through the matrix pores, due to a major influence on pore size,

Table 5
MOR, LOP, MOE, and specific toughness (I_G) values of composite samples cured in a CO_2 chamber under different time and moisture content conditions. The values in brackets correspond to standard deviations (SD). The letters in italics indicate the significance groups obtained from the Tukey test.

Sample ref.	Moisture content	Curing days	MOR (MPa)	LOP (MPa)	MOE (MPa)	I_G (kJ/m^2)	MOR/LOP ratio
CLMK/Flax-0/7	0%	7	3.17 (0.51) *bc*	2.03 (0.36) *b*	0.18 (0.05) *de*	3.27 (0.93) *de*	1.56
CLMK/Flax-0/14		14	4.26 (1.09) *b*	2.48 (0.44) *b*	0.28 (0.05) *bc*	4.47 (0.82) *cd*	1.72
CLMK/Flax-33/7	33%	7	5.63 (0.20) *a*	4.58 (0.42) *a*	0.26 (0.04) *bcd*	4.86 (0.63) *bcd*	1.23
CLMK/Flax-33/14		14	5.80 (0.73) *a*	4.25 (0.36) *a*	0.31 (0.05) *bc*	5.53 (0.88) *abc*	1.36
CLMK/Flax-66/7	66%	7	5.70 (0.50) *a*	4.90 (0.91) *a*	0.32 (0.05) *b*	6.43 (1.12) *ab*	1.16
CLMK/Flax-66/14		14	5.81 (0.94) *a*	4.17 (0.75) *a*	0.46 (0.05) *a*	6.88 (1.91) *a*	1.39
CLMK/Flax-100/7	100%	7	2.77 (0.29) *c*	2.10 (0.38) *b*	0.13 (0.03) *e*	2.45 (0.29) *e*	1.32
CLMK/Flax-100/14		14	3.44 (0.15) *bc*	2.00 (0.37) *b*	0.23 (0.05) *cd*	3.77 (0.59) *cde*	1.72

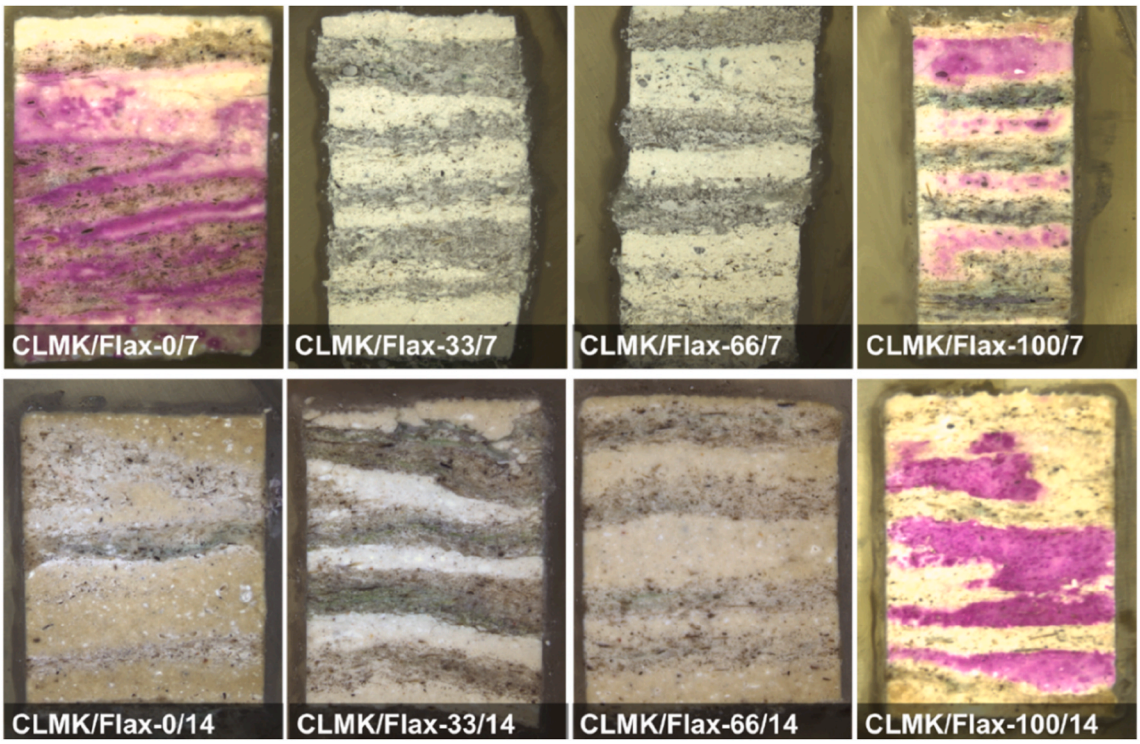

Fig. 6. Optical images of samples cured for 7 days (top) and 14 days (bottom).

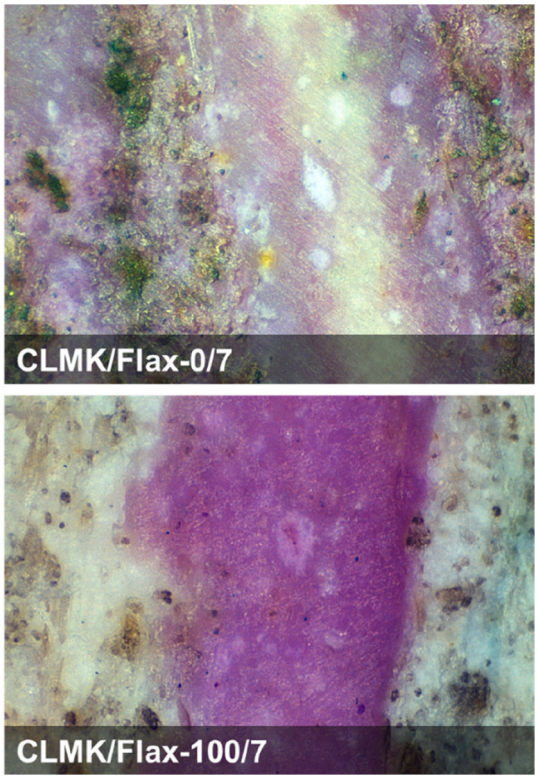

Fig. 7. Optical microscopy (100x) of the samples with low moisture (left) and high moisture (right) cured in a CO_2 chamber for 7 days.

in both gaseous (air) and liquid (water) media, although the former is faster. In fact, if the pore is saturated with water, the rate of CO_2 diffusion is between 4 and 5 orders of magnitude slower [37,38]. In addition to the CO_2 diffused into the matrix, a certain degree of humidity is also required to generate the carbonic acid necessary for the reaction. The carbonic acid then combines with Ca ions, producing calcium carbonate from the desorption of calcium hydroxide. This desorption, in turn, liberates more water into the media. Thus, carbonation depends on the balance between the diffusivity of the CO_2 through the unsaturated pores of the lime paste and the moisture content required to produce the reaction. However, the carbonation reaction can also be initiated under conditions of no humidity through the combination and direct desorption of the calcium hydroxide with CO_2. This reaction, although much slower than the previously described one, also produces humidity as a result [36]. In this case, the reaction is also capable of carbonating the C–S–H [39].

As for the role of the fibres, it should be noted that, despite the hornification treatment applied, the reinforcement fabric used continues to have a greater capacity for water absorption and retention than the matrix. This is due to the nature (chemical composition) of its fibres. Moreover, they also have a tubular structure (lumen) that permits the transmission of gases and fluids from end to end of the fibre.

Thus, we may hypothesise that the fibres of the reinforcement fabric play a key role in moisture retention, and also in CO_2 and water transport across the material. Fig. 8 reveals a scheme of the possible interaction in samples of low and high moisture content during plate curing, considering both the air extraction step (phase vacuum), and the CO_2 gas injection step (phase CO_2).

For the sample having a low moisture content, in the air extraction phase, the low moisture content available could be forced out with a vacuum, mainly through the tubular fibre structure. Then, during the CO_2 injection phase, a good diffusion of the gas is achieved throughout the specimen, due to the material's high porosity, since both fibres and matrix pores are not saturated with moisture. In this case, the carbonation reaction would be initiated according to the aforementioned direct carbonation reaction, which is produced under no-humidity conditions and generates a certain humidity. This reaction would boost the carbonation process in the central matrix areas, according to the previously explained typical reaction. However, in the areas surrounding the fibres, the water generated by this direct carbonation reaction would

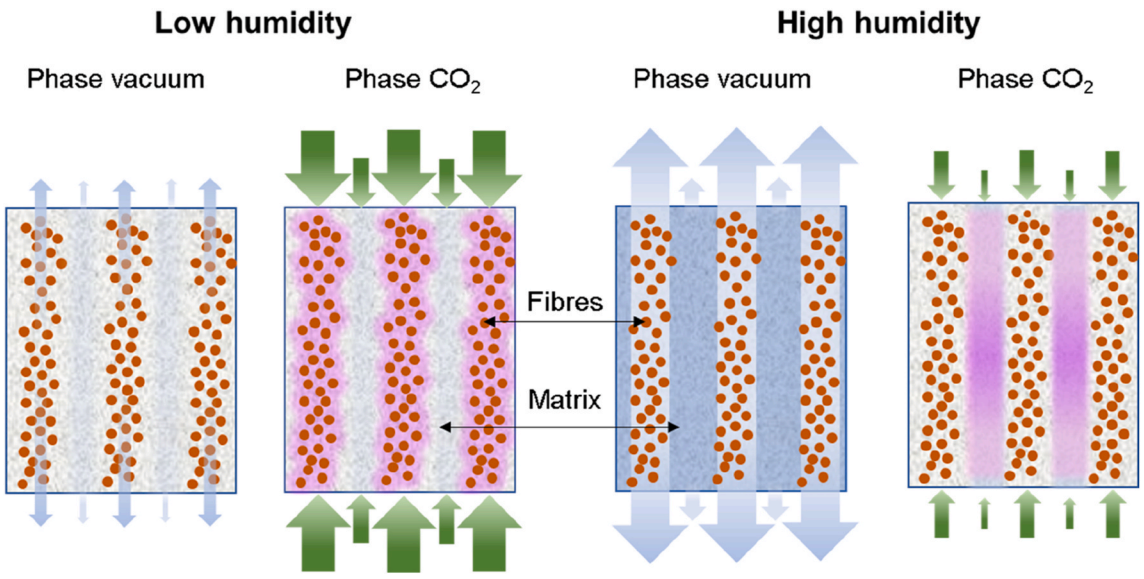

Fig. 8. Scheme of the influence of the fibres in the material's carbonation for low and high moisture. Moisture is represented in blue, CO_2 in green, and phenolphthalein staining in purple. Note that the arrow sizes are significant. (For interpretation of the references to colour in this figure legend, the reader is referred to the Web version of this article.)

be reabsorbed by these fibres, avoiding the propagation of the typical carbonation reaction. Thus, the limited direct carbonation, which occurs at a lower speed, could only reach the sample carbonation after 14 days (see Fig. 6, CLMK/Flax-0/7 vs CLMK/Flax-0/14).

In the case of the high moisture sample, the removal of water in the air extraction phase is greater and much faster across the fibre's lumen than through the porous matrix. This results in the desaturation of the fibre's lumen, despite the normally high moisture retention maintained across the fibre walls, while the matrix continues to be mainly saturated. Therefore, in the CO_2 injection phase, the fibre's lumens may act as

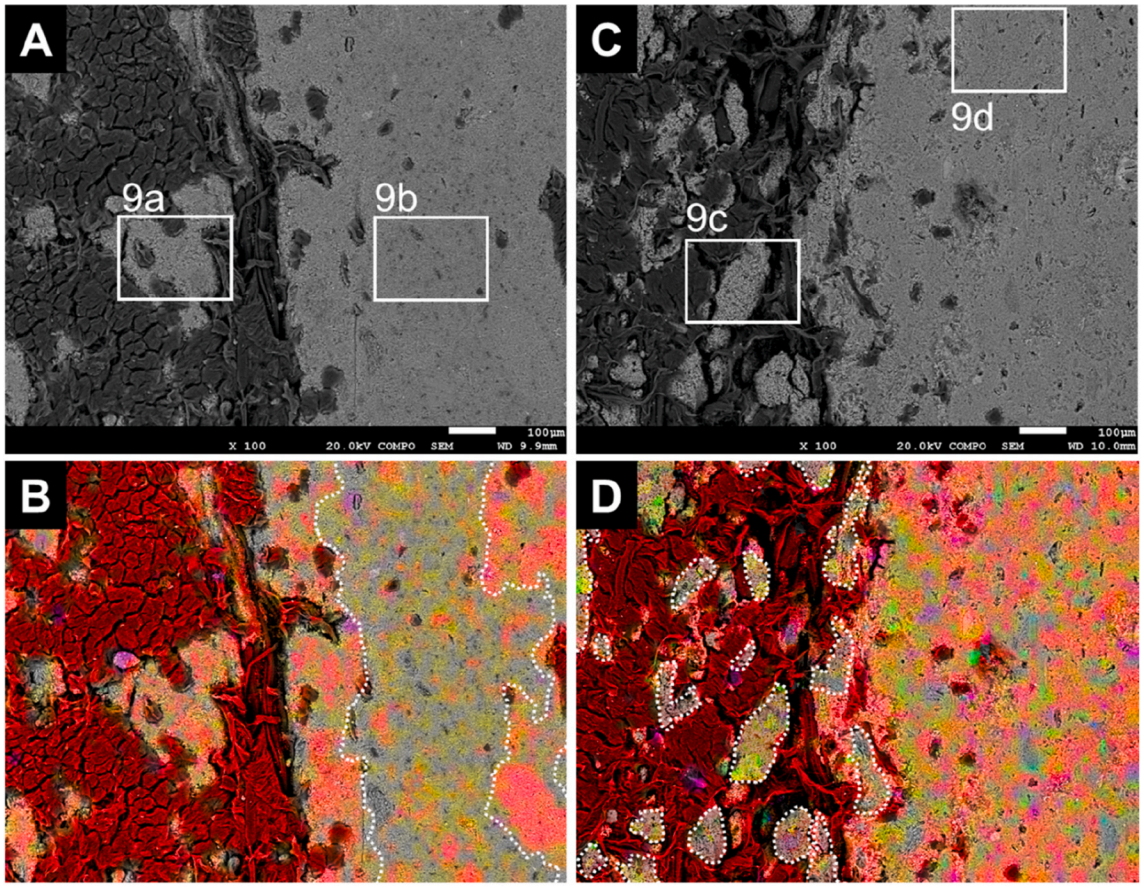

Fig. 9. *BSEM imaging (A and C) and layered EDS maps (B and D) of the samples cured in a CO2 chamber for 7 days at low moisture (A and B) and high moisture (C and D). In B and D, white dotted lines delimit carbonated areas. Please note that areas marked in 8A and 8C are analysed in* Fig. 9. Scale bars correspond to 100 µm.

channels for CO_2 transport, whereas the diffusion capacity of the gas in the matrix will be very low given the water saturation of the pores. Thanks to the non-saturated moisture lumen channel, the fibres would have greatly contributed to the CO_2 diffusion, meaning that, together with the retained moisture, the carbonation of the matrix adjacent to this area would have taken place. However, the water saturation in the matrix pores would have considerably limited the carbonation, which could not be reached even at 14 days (see Fig. 6, CLMK/Flax-100/14 and also CLMK/Flax-100/7).

3.2.2. *Effect of fibres and moisture content on the lime/flax composite's microstructure*

Continuing the in-depth analysis of the carbonation process of the samples with extreme moisture contents cured for 7 days, the microstructure of the samples CLMK/Flax-0/7 (0% moisture content, left) and CLMK/Flax-100/7 (100% moisture content, right) was analysed via electron microscopy (see Fig. 9).

Fig. 9A and C correspond to the BSEM images, revealing a limited penetrability of the lime matrix into the fabric, reaching only the outer fibres. Moreover, it is also evident that regardless of the degree of carbonation, the matrix's microstructure differs depending on its distance to the fibres. Being close to the fibres, the matrix appears to be more porous than in the central areas, where it appears to be more compact.

Fig. 9B and D correspond to the layered EDS maps for the same areas as 9A and 9C respectively, obtained through an EDS analysis of Ca (red), Si (blue), and Al (green) ions. As highlighted in these images, the map of elements shows a colour alteration in the matrix. This is due to the proportional variation of the Ca, Si and Al ions, resulting from the carbonation and pozzolanic reactions. The proportional variation of the Ca ion is produced by the transformation of calcium hydroxide and C–S–H into calcium carbonate through the carbonation process. However, both images reveal the presence of green spots corresponding to the Al ion coming from MK particles. In this case, its proportional variation is produced by the MK combination with calcium hydroxide to form C–S–H, which also causes a proportional variation in the Si ion (blue). Finally, depending on the concentration of C–S–H with respect to Ca (either in the form of hydroxide or carbonate), different shades of magenta may be seen. This change is consistent with the optical imaging results shown previously.

3.2.3. *Chemical composition*

Fig. 10 presents the layered EDS map of the areas detailed in Fig. 9A and C, where the images on the left correspond to the sample at a low moisture content, and the images on the right correspond to the sample at a high moisture content.

From the point of view of the chemical composition, in Fig. 10a (matrix between fibres), the reddish colouration is identified as non-carbonated and corresponds to the area with the highest proportion of calcium as compared to the other elements. There is also a specific amount of light green of the Al ion, and some blurry magenta areas, representing the mixture of the blue of the silicon ion and the red of the Ca identified with the C–S–H. Fig. 10b offers a detailed look at the carbonated matrix area (matrix in the lime layer), where instead of the red colouration, the following may be observed: (i) a spreading pattern of pink areas of calcium hydroxide, (ii) C–S–H magenta areas, (iii) a few undissolved remnants of metakaolin – which appear in turquoise as a result of the mixture of Al (green) and Si (blue) ions –, and (iv) a large

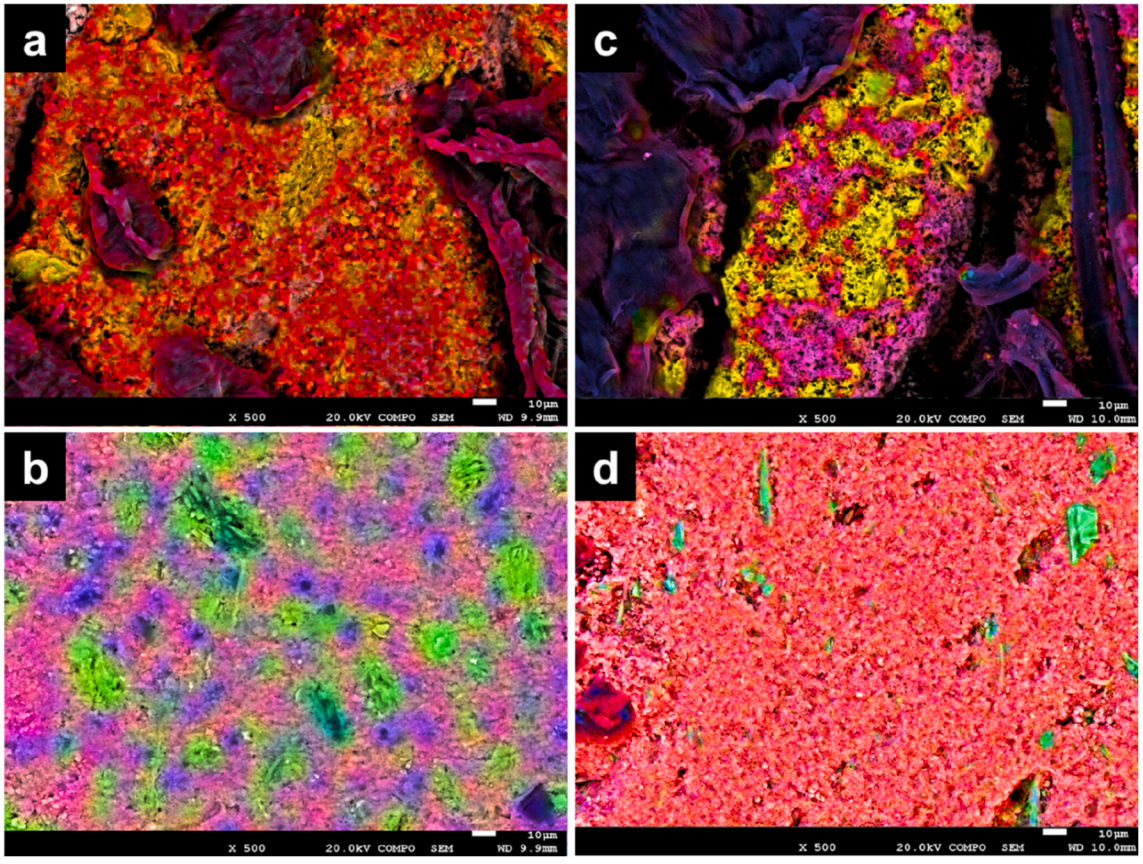

Fig. 10. Detailed layered EDS map of the areas indicated in Fig. 9A and C, corresponding to: (a) matrix between fibres area, cured at low moisture, not carbonated; (b) matrix area, cured at low moisture, carbonated; (c) matrix between fibres area, cured at high moisture, carbonated; (d) matrix area, cured at high moisture, not carbonated. Colours correspond to Ca (red), Al (light green) and Si (dark blue). Scale bars correspond to 10 µm. (For interpretation of the references to colour in this figure legend, the reader is referred to the Web version of this article.)

amount of light green areas of silicon-impoverished metakaolin particles.

Fig. 10c presents information about the matrix area located between the fibres of the reinforcement, with a light green colouration of the Al ion, and numerous magenta areas that correspond to C–S–H and are, in turn, surrounded by reddish boundaries identified as calcium hydroxide. Fig. 10d shows the central part of the non-carbonated matrix in the lime layer, which mainly has a red colouration identified as calcium hydroxide, with some magenta areas of the C–S–H, and a few turquoise spots corresponding to the MK particles.

3.2.4. Physical microstructure

From a microstructural point of view, the differences in particle shape are determined by the polymorphism of the precipitated calcite crystals as well as the morphology of the C–S–H phases generated from the pozzolanic reactions. The precipitation of hydrated material depends on numerous parameters, such as the concentration of CO_2 and moisture content, both of which are related to the reaction rate [40]. Thus, the following may be found: (i) amorphous formations of $CaCO_3$, (ii) chains of calcite nanocrystals – generated at the onset of the carbonation reaction and precipitated directly on the portlandite crystals –, (iii) amorphous or nanostructured C–S–H precipitate – precipitated on portlandite crystals –, and (iv) calcite crystals of scalenohedral or rhombohedral shape – produced by dissolution and recrystallisation of calcite from other mineral phases – [41]. Moreover, due to the composition of the matrix, undissolved particles of the metakaolin, used as pozzolanic

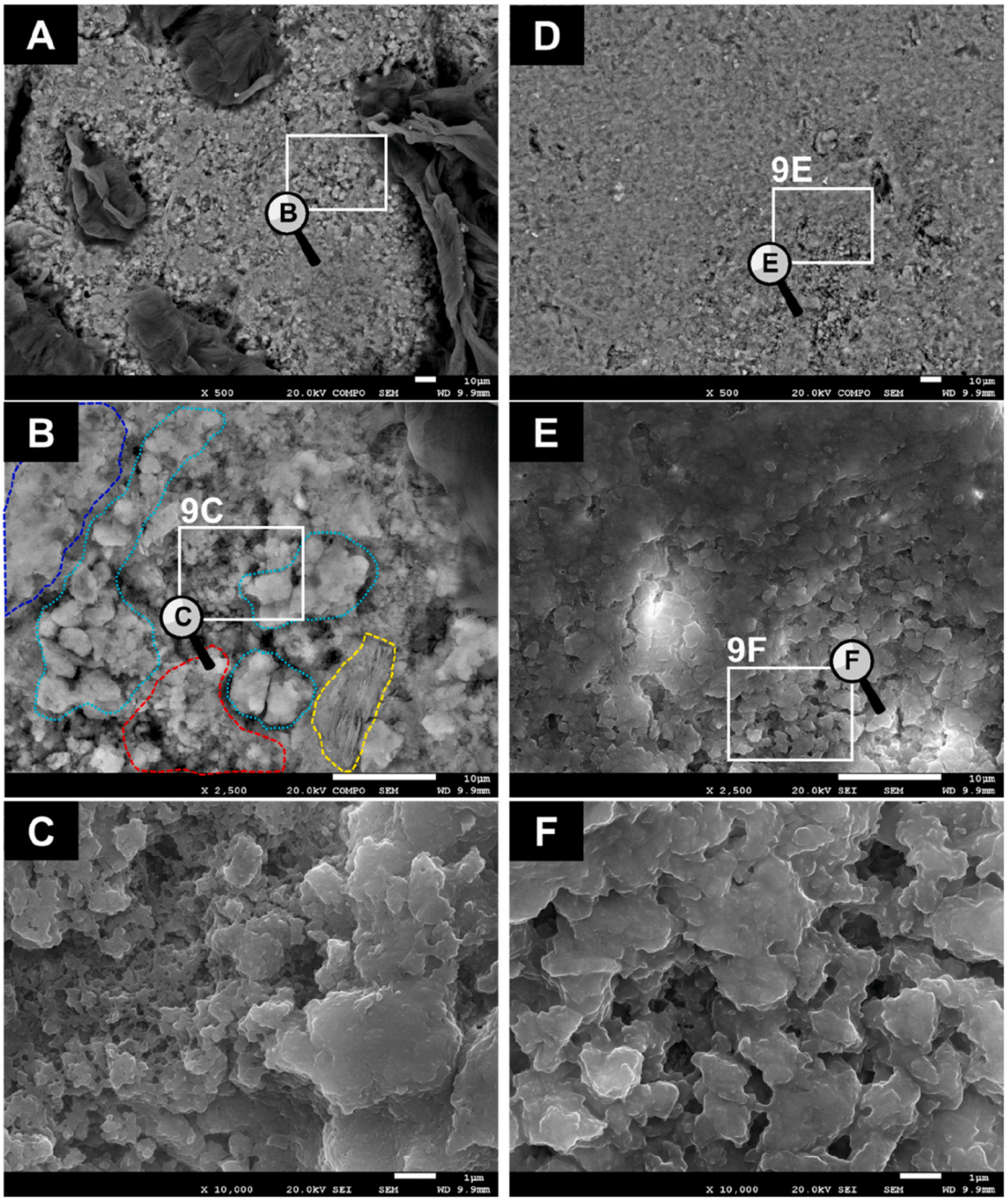

Fig. 11. *Detail of the sample CLMK/Flax-0/7. Images on the left (A, B and C) correspond to the matrix microstructure near the fibres; and images on the right (D, E and F) correspond to the matrix microstructure in an area significantly far from the fibres. Scale bars correspond to* 10 µm *in A, B, D and E; and* 1 µm *in C and F.*

material, can also be found. Figs. 11 and 12 show details of the microstructures for the same areas analysed in Fig. 10.

Fig. 11 corresponds to the CLMK/Flax-0/7 sample, presenting the microstructure of the matrix in the areas next to the fibres (left, Fig. 11A, B and 11C) and in the central matrix areas (right, Fig. 11D, E and 11F).

Fig. 11A reveals that the matrix surrounding the fibres has a higher porosity and a larger particle size than in the central areas (sufficiently separated from the areas with fibres). Different particle morphologies are shown in detail in Fig. 11B: (i) a semi-dissolved MK particle (yellow dashed line), with the characteristic nanometric sheets; (ii) clusters of portlandite microcrystals on which amorphous C–S–H layers (dotted blue line) have precipitated; (iii) large areas of portlandite microcrystals (red dashed line); and (iv) areas of C–S–H amorphous gel (dark blue dashed line). Fig. 11C reveals that the pores are full of nano-sized C–S–H amorphous precipitates.

Moreover, Fig. 11D shows a much more compact and homogeneous matrix. The information in Fig. 11E reveals that the structure is composed mainly of calcium carbonate in the form of microcrystals, coated with amorphous precipitates (probably of carbonated C–S–H). In the more porous areas (Fig. 11F), the morphology is similar to that of Fig. 11C, but with larger and more dispersed pores, resulting in a less intricate structure.

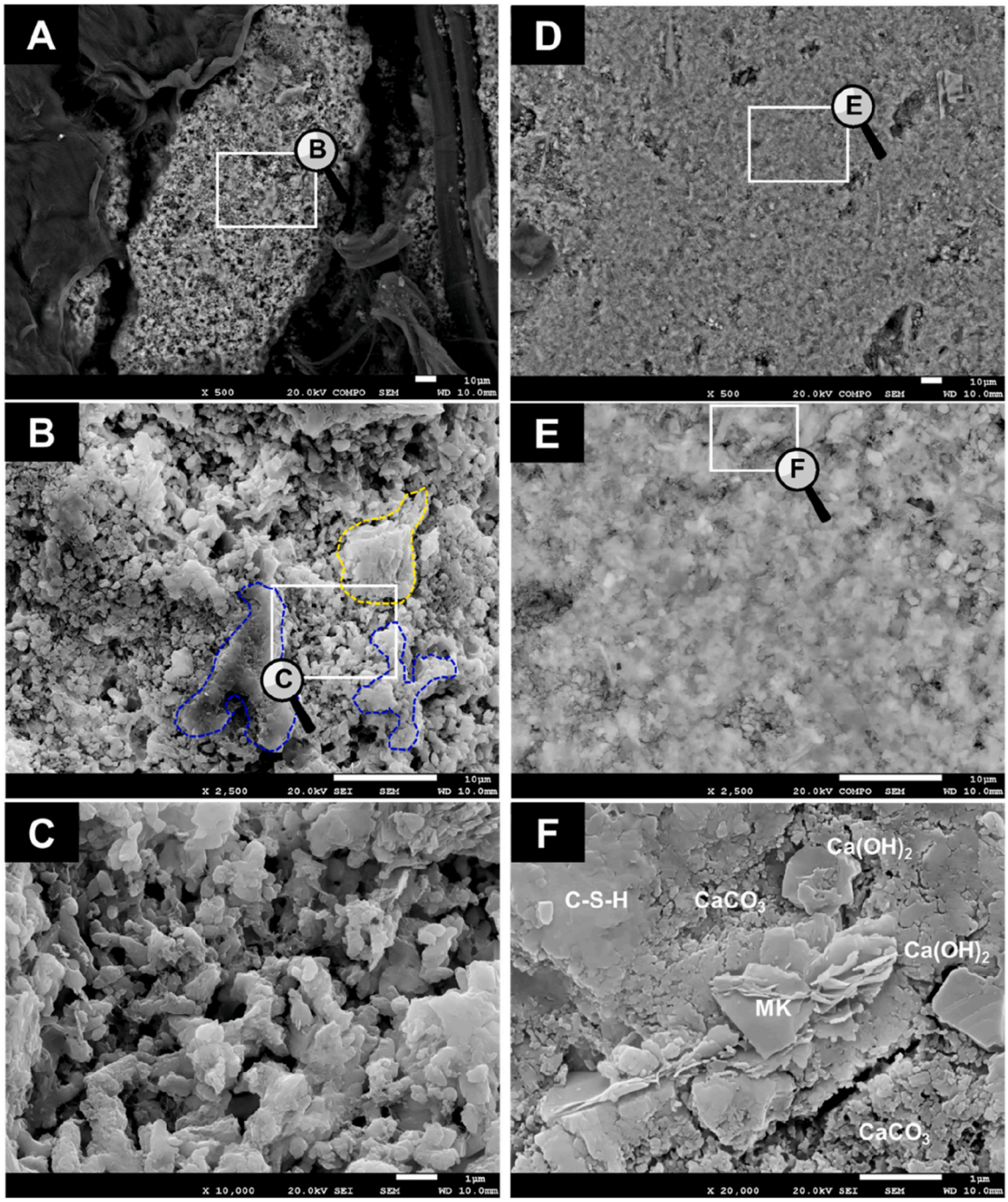

Fig. 12. *Details of the CLMK/Flax-100/7 sample. Images on the left (A, B and C) correspond to the matrix microstructure near the fibres; and images on the right (D, E and F) correspond to the matrix microstructure in an area significantly distanced from the fibres. Blue dashed lines correspond to remnants of MK particles, and yellow dashed lines correspond to decalcified phases of C–S–H. Scale bars correspond to* 10 µm *in A, B, D and E; and* 1 µm *in C and F.* (For interpretation of the references to colour in this figure legend, the reader is referred to the Web version of this article.)

Fig. 12 presents a detailed look at the different matrix areas of the CLMK/Flax-100/7 sample. Compared to those with low moisture, the matrix between fibres has a more granular and porous topography (Fig. 12A). Fig. 12B contains mainly calcite microcrystals, a few laminar remains of MK particles (yellow dashed line), and some amorphous areas that may correspond to the decalcified phases of C–S–H (dark blue dashed line). Calcite crystals are shown in detail in Fig. 12C, revealing a high but scattered nucleation, since a high porosity can be observed. This may be due to an excess of water present during the curing, which may cause the dissolution and combination of calcium hydroxide and its further precipitation in calcium carbonate form.

As for the matrix found in the lime layer, Fig. 12D shows a general microstructure that is similar to that of the very compact Fig. 11D. The information provided in Fig. 12E reveals that the microstructure is mainly calcium hydroxide crystals covered in C–S–H gel, but also with nanocrystals that may correspond to calcite ($CaCO_3$) or C–S–H, and a few MK particles. In this case, the C–S–H gel fills the gaps between the calcium hydroxide particles.

The differences observed in the microstructure of the matrix according to its proximity to the fibres corroborate the relevant role of the fibres in the carbonation process under extreme conditions. Fibre reinforcement layers regulate the amount of moisture in the environment and actively participate in the transport and diffusion of water and CO_2. It has been shown that the resulting microstructure in the matrix between fibres is more porous than the matrix in the lime layers, with the pores of the 100% moisture content sample being larger. It is worth mentioning that porosity also plays a major role in the material's mechanical properties, where higher porosities result in lower mechanical performance.

In summary, the results observed in this microstructural analysis involving carbonation and porosity (section 3.2) are consistent with the flexural behaviour found in the analysis of mechanical properties (section 3.1).

4. Conclusions

This paper examines the influence of moisture content, the time of exposure to high concentrations of CO_2 and the incorporation of vegetable fibres on the mechanical properties, as well as the extent of carbonation and microstructure of lime-based composite reinforced by non-woven flax fabrics used for masonry reinforcement in historical structures. The following are the main findings of the study.

- The mechanical properties of the lime composites were found to increase with the matrix carbonation. While 7 days are enough to acquire a good flexural strength, longer carbonation times (14 days) are needed to improve the stiffness.
- Despite the carbonation is necessary to obtain good mechanical performance, all composite materials presented a high tenacity with a strain-hardening behaviour.
- The reinforcement of vegetable fibres was efficient under any of the study conditions, helping to maintain a good ductility of the composite material.
- Based on the phenolphthalein test, the samples cured for 7 days with 33% and 66% moisture content, and those cured for 14 days with 0%, 33% and 66% moisture content presented very high or complete carbonation.
- Optimal curing conditions were found to be the intermediate moisture contents (66% being ideal) and larger exposure times (14 days being ideal), although the best trade-off between mechanical properties and production costs was found for the CLMK/Flax-66/7 sample (curing with 66% of moisture content for 7 days).
- The fibres also appeared to play a relevant role in the carbonation process for the samples with extreme moisture contents, participating in the transport and diffusion of water and CO_2.
- At low moisture conditions (0%), fibres absorb any available humidity, allowing matrix carbonation only through a direct desorption mechanism. However, at high moisture conditions (100%) the fibres enhance the water and CO_2 diffusion, leading to the complete carbonation of the matrix surrounding the fibres.
- Fibres present a relevant effect on the paste microstructure owing to their interaction with water regardless the humidity content of the material. The lime paste surrounding the fibres presented a higher porosity and larger particles, whereas the matrix in areas significantly distanced from the fibres present a more homogenous and denser microstructure with smaller particles.

Declaration of competing interest

The authors declare that they have no known competing financial interests or personal relationships that could have appeared to influence the work reported in this paper.

Data availability

Data will be made available on request.

Acknowledgements

This work was supported through the project grant PID2019-108067RB-I00/AEI/10.13039/501100011033 by the Ministerio de Ciencia e Innovación (MCIN)/Agencia Estatal de Investigación (AEI) of the Spanish Government. The author Heura Ventura is a Serra-Húnter fellow.

References

[1] S.M. Cascone, V. Sapienza, I. Lionti, S.M. Carmela Porto, Fiber-reinforced polymer nets for strengthening lava stone masonries in historical buildings, Sustain. Times 8 (2016), https://doi.org/10.3390/su8040394.
[2] F. Iucolano, B. Liguori, C. Colella, Fibre-reinforced lime-based mortars: a possible resource for ancient masonry restoration, Construct. Build. Mater. 38 (2013) 785–789, https://doi.org/10.1016/j.conbuildmat.2012.09.050.
[3] M. del M. Barbero-Barrera, L. Maldonado-Ramos, K. Van Balen, A. García-Santos, F. J. Neila-González, Lime render layers: an overview of their properties, J. Cult. Herit. 15 (2014) 326–330, https://doi.org/10.1016/j.culher.2013.07.004.
[4] G. Lorenzo, Q. Enrico, D. Marco, New approaches to building pathology and durability, New Approaches to Build. Pathol. Durab. 6 (2016) 159–175, https://doi.org/10.1007/978-981-10-0648-7.
[5] B.A. Silva, A.P. Ferreira Pinto, A. Gomes, Natural hydraulic lime versus cement for blended lime mortars for restoration works, Construct. Build. Mater. 94 (2015) 346–360, https://doi.org/10.1016/j.conbuildmat.2015.06.058.
[6] A. Moropoulou, A. Bakolas, S. Anagnostopoulou, Composite materials in ancient structures, Cem. Concr. Compos. 27 (2005) 295–300, https://doi.org/10.1016/j.cemconcomp.2004.02.018.
[7] G. Ferrara, M. Pepe, E. Martinelli, R.D. Tolêdo Filho, Tensile behavior of flax textile reinforced lime-mortar: influence of reinforcement amount and textile impregnation, Cem. Concr. Compos. 119 (2021), 103984, https://doi.org/10.1016/j.cemconcomp.2021.103984.
[8] P. Sadrolodabaee, Sustainability, durability and mechanical characterization of a new recycled textile-reinforced strain-hardening cementitious composite for building applications, Dr. Thesis ,UPC-BarcelonaTECH (2022), https://doi.org/10.13140/RG.2.2.11814.19524.
[9] J. Wei, C. Meyer, Improving degradation resistance of sisal fiber in concrete through fiber surface treatment, Appl. Surf. Sci. 289 (2014) 511–523, https://doi.org/10.1016/j.apsusc.2013.11.024.
[10] M. Ardanuy, J. Claramunt, R.D. Toledo Filho, Cellulosic fiber reinforced cement-based composites: a review of recent research, Construct. Build. Mater. 79 (2015) 115–128, https://doi.org/10.1016/j.conbuildmat.2015.01.035.
[11] P. Sadrolodabaee, J. Claramunt, M. Ardanuy, A. de la Fuente, Mechanical and durability characterization of a new textile waste micro-fiber reinforced cement composite for building applications, Case Stud. Constr. Mater. 14 (2021), e00492, https://doi.org/10.1016/j.cscm.2021.e00492.
[12] P. Sadrolodabaee, J. Claramunt Blanes, M. Ardanuy Raso, A. de la Fuente Antequera, Preliminary study on new micro textile waste fiber reinforced cement composite, in: ICBBM 2021 4th Int. Conf. Bio-Based Build. Mater. Barcelona, 2021, pp. 37–42. Catalunya June 16-18, 2021 Proc.
[13] P. Sadrolodabaee, J. Claramunt, M. Ardanuy, A. De La Fuente, Materials A textile waste fiber-reinforced cement composite: comparison between short random fiber and textile reinforcement, 3742. 14, Materials 14 (2021) 3742, https://doi.org/10.3390/ma14133742, 2021.

[14] P. Sadrolodabaee, S.M.A. Hosseini, M. Ardunay, J. Claramunt, A. de la Fuente, A New Sustainability Assessment Method for Façade Cladding Panels: A Case Study of Fiber/Textile Reinforced Cement Sheets, 2021, pp. 809–819, https://doi.org/10.1007/978-3-030-83719-8_69.
[15] P. Sadrolodabaee, J. Claramunt, M. Ardanuy, A. de la Fuente, Effect of accelerated aging and silica fume addition on the mechanical and microstructural properties of hybrid textile waste-flax fabric-reinforced cement composites, Cem. Concr. Compos. 135 (2023), 104829, https://doi.org/10.1016/J.CEMCONCOMP.2022.104829.
[16] B. Mobasher, Mechanics of fiber and textile reinforced cement composites, 2011. https://doi.org/10.1201/b11181.
[17] L. Gonzalez-Lopez, J. Claramunt, L. Haurie, H. Ventura, M. Ardanuy, Study of the fire and thermal behaviour of façade panels made of natural fibre-reinforced cement-based composites, Construct. Build. Mater. 302 (2021), 124195, https://doi.org/10.1016/J.CONBUILDMAT.2021.124195.
[18] P. Sadrolodabaee, J. Claramunt, M. Ardanuy, A. de la Fuente, Characterization of a textile waste nonwoven fabric reinforced cement composite for non-structural building components, Construct. Build. Mater. 276 (2021), 122179, https://doi.org/10.1016/j.conbuildmat.2020.122179.
[19] A. Rakhsh Mahpour, M. Ardanuy Raso, H. Ventura Casellas, J.R. Rosell Amigó, J. Claramunt Blanes, Rheology, mechanical performance and penetrability through flax nonwoven fabrics of lime pastes, Proc. 4th Int. Conf. Bio-Based Build. Mater. (2021) 639–647. https://upcommons.upc.edu/handle/2117/348017#.YTJqdc2wENc.mendeley. (Accessed 3 September 2021). accessed.
[20] P. Sadrolodabaee, S.M.A. Hosseini, J. Claramunt, M. Ardanuy, L. Haurie, A. M. Lacasta, A. de la Fuente, Experimental characterization of comfort performance parameters and multi-criteria sustainability assessment of recycled textile-reinforced cement facade cladding, J. Clean. Prod. 356 (2022), 131900, https://doi.org/10.1016/J.JCLEPRO.2022.131900.
[21] R. Infante Gomes, C. Brazão Farinha, R. Veiga, J. de Brito, P. Faria, D. Bastos, CO2 sequestration by construction and demolition waste aggregates and effect on mortars and concrete performance - an overview, Renew. Sustain. Energy Rev. 152 (2021), 111668, https://doi.org/10.1016/J.RSER.2021.111668.
[22] M. Arandigoyen, J.I. Alvarez, Pore structure and mechanical properties of cement–lime mortars, Cement Concr. Res. 37 (2007) 767–775, https://doi.org/10.1016/J.CEMCONRES.2007.02.023.
[23] D. Ergenç, R. Fort, Accelerating carbonation in lime-based mortar in high CO2 environments, Construct. Build. Mater. 188 (2018) 314–325, https://doi.org/10.1016/j.conbuildmat.2018.08.125.
[24] A. Sepulcre-Aguilar, F. Hernández-Olivares, Assessment of phase formation in lime-based mortars with added metakaolin, Portland cement and sepiolite, for grouting of historic masonry, Cement Concr. Res. 40 (2010) 66–76, https://doi.org/10.1016/j.cemconres.2009.08.028.
[25] K.L. Konan, C. Peyratout, A. Smith, J.P. Bonnet, S. Rossignol, S. Oyetola, Comparison of surface properties between kaolin and metakaolin in concentrated lime solutions, J. Colloid Interface Sci. 339 (2009) 103–109, https://doi.org/10.1016/j.jcis.2009.07.019.
[26] H. Ventura, M. Ardanuy, X. Capdevila, F. Cano, J.A. Tornero, Effects of needling parameters on some structural and physico-mechanical properties of needle-punched nonwovens, J. Text. Inst. 105 (2014) 1065–1075, https://doi.org/10.1080/00405000.2013.874628.
[27] J. Claramunt, L. Fernández-Carrasco, H. Ventura, M. Ardanuy, Natural fiber nonwoven reinforced cement composites as sustainable materials for building envelopes, Construct. Build. Mater. 115 (2016) 230–239, https://doi.org/10.1016/j.conbuildmat.2016.04.044.
[28] U. Weise, H. Paulapuro, Effect of drying and rewetting cycles on fibre swelling, J. Pulp Pap. Sci. 25 (1999) 163–166.
[29] M. Ardanuy, J. Clarmunt, Influence of the hornification process of cellulosic fibres on resistance of cementitious composites, Tech. Text. (2010) 16–18.
[30] J.E.M. Ballesteros, V. dos Santos, G. Mármol, M. Frías, J. Fiorelli, Potential of the hornification treatment on eucalyptus and pine fibers for fiber-cement applications, Cellulose 24 (2017) 2275–2286, https://doi.org/10.1007/s10570-017-1253-6.
[31] J. Claramunt, M. Ardanuy, J.A. García-Hortal, Effect of drying and rewetting cycles on the structure and physicochemical characteristics of softwood fibres for reinforcement of cementitious composites, Carbohydr. Polym. 79 (2010) 200–205, https://doi.org/10.1016/j.carbpol.2009.07.057.
[32] M. Ardanuy, J. Claramunt, H. Perron, H. Ventura, A.M. Manich, Effects of drying and rewetting cycles on the water absorption of vegetable fibres for composite reinforcement, in: Congr. Biobased Mater. Nat. Fibres WPC, 2014.
[33] J. Claramunt Blanes, M. Ardanuy Raso, J.A. García Hortal, A. Clemente Escuin, Effect of Drying and Rewetting Cycles of Cellulosic Fibres on Resistance of Cementitious Composites, vol. 25, 2009, 11302. http://upcommons.upc.edu/e-prints/handle/2117/6356.
[34] J.E.M. Ballesteros, S.F. Santos, G. Mármol, H. Savastano, J. Fiorelli, Evaluation of cellulosic pulps treated by hornification as reinforcement of cementitious composites, Construct. Build. Mater. 100 (2015) 83–90, https://doi.org/10.1016/j.conbuildmat.2015.09.044.
[35] RILEM, The determinarion of energy absortion in flexure of thin fibre reinforced cement sections, Mater. Struct. 17 (1984) 171–173.
[36] M. Arandigoyen, J.I. Álvarez, Carbonation process in lime pastes with different water/binder ratio, Mater. Construcción 56 (2006) 5–18, https://doi.org/10.3989/mc.2006.v56.i281.88.
[37] K. Van Balen, Carbonation reaction of lime, kinetics at ambient temperature, Cement Concr. Res. 35 (2005) 647–657, https://doi.org/10.1016/j.cemconres.2004.06.020.
[38] K. Van Balen, D. Van Gemert, Modelling lime mortar carbonation, Mater. Struct. 27 (1994) 393–398, https://doi.org/10.1007/BF02473442.
[39] H.F.W. Taylor, Cement Chemistry, T. Telford, London, 1997.
[40] Ö. Cizer, K. Van Balen, J. Elsen, D. Van Gemert, Real-time investigation of reaction rate and mineral phase modifications of lime carbonation, Construct. Build. Mater. 35 (2012) 741–751, https://doi.org/10.1016/j.conbuildmat.2012.04.036.
[41] Ö. Cizer, C. Rodriguez-Navarro, E. Ruiz-Agudo, J. Elsen, D. Van Gemert, K. Van Balen, Phase and morphology evolution of calcium carbonate precipitated by carbonation of hydrated lime, J. Mater. Sci. 47 (2012) 6151–6165, https://doi.org/10.1007/s10853-012-6535-7.